

Quantum-Inspired Tensor Networks for Approximating PDE Flow Maps

Nahid Binandeh Dehaghani, Ban Q. Tran, Rafal Wisniewski, Susan Mengel, and A. Pedro Aguiar

Abstract—We investigate quantum-inspired tensor networks (QTNs) for approximating flow maps of hydrodynamic partial differential equations (PDEs). Motivated by the effective low-rank structure that emerges after tensorization of discretized transport and diffusion dynamics, we encode PDE states as matrix product states (MPS) and represent the evolution operator as a structured low-rank matrix product operator (MPO) in tensor-train form (e.g., arising from finite-difference discretizations assembled in MPO form). The MPO is applied directly in MPS form, and rank growth is controlled via canonicalization and SVD-based truncation after each step. We provide theoretical context through standard matrix product properties, including exact MPS representability bounds, local optimality of SVD truncation, and a Lipschitz-type multi-step error propagation estimate. Experiments on one- and two-dimensional linear advection-diffusion and nonlinear viscous Burgers equations demonstrate accurate short-horizon prediction, favorable scaling in smooth diffusive regimes, and error growth in nonlinear multi-step predictions.

I. INTRODUCTION

Hydrodynamic partial differential equations (PDEs) governing transport and diffusion arise across fluid dynamics, materials transport, and nonlinear wave propagation. Although structurally simple, such equations can develop sharp gradients, multiscale interactions, and sensitivity to perturbations, making accurate and scalable numerical simulation increasingly challenging as spatial resolution and dimension increase.

An alternative to classical discretization-based solvers is to approximate the discrete-time *flow map* that advances the state over a fixed time step. This viewpoint is closely related to Koopman/operator perspectives [1], [2], where dynamics are represented through linear operators acting on high-dimensional state spaces. However, for spatially discretized PDEs the state dimension grows exponentially with resolution, rendering naive operator representations and applications computationally infeasible.

Tensor network representations provide a principled mechanism for mitigating this curse of dimensionality. Originally developed in quantum many-body physics [3], [4],

Nahid Binandeh Dehaghani is with the Department of Electronic Systems, Aalborg University, Aalborg, Denmark. nahidbd@es.aau.dk

Ban Q. Tran is with the Department of Computer Science, Texas Tech University, Lubbock, USA, and Department of Computing Fundamentals, FPT University, Hanoi, Vietnam. bantran@ttu.edu – bantran@fpt.edu.vn

Rafal Wisniewski is with the Department of Electronic Systems, Aalborg University, Aalborg, Denmark. raf@es.aau.dk

Susan Mengel is with the Department of Computer Science, Texas Tech University, Lubbock, USA. susan.mengel@ttu.edu

A. Pedro Aguiar is with SYSTEC-ARISE, Faculty of Engineering, University of Porto, Porto, Portugal. pedro.aguiar@fe.up.pt

tensor networks exploit low-rank structure to represent high-dimensional states and operators efficiently. In particular, matrix product states (MPS), also known as tensor trains [4], [5], admit representations whose complexity scales linearly with dimension when correlations remain sufficiently localized. Such quantum-inspired representations have increasingly been adopted in classical scientific computing for compression and structured operator approximation [6], [7], [8], [9]. Throughout, *QTN* refers to the quantum-inspired tensor-network framework instantiated with MPS (tensor trains) for states and matrix product operator (MPO) for operators.

Many transport-dominated PDEs exhibit effective low-rank structure over finite time horizons: smooth initial data, diffusive effects, and locality of interactions tend to limit long-range correlations in discretized states [7], [8], [9]. This suggests that PDE flow maps may admit compact tensor-network representations. At the same time, nonlinear dynamics can generate complex correlations that challenge low-rank approximations, motivating a systematic study of both the capabilities and limitations of tensor-network time stepping. We make the following contributions:

- We investigate a quantum-inspired tensor network framework for approximating PDE flow maps, representing states as MPS and evolution operators as low-rank MPOs in tensor-train form.
- We provide theoretical context grounded in standard matrix product properties, including exact MPS representability bounds, optimality of SVD-based truncation, and a Lipschitz-type multi-step error propagation estimate.
- We perform systematic numerical experiments on linear and nonlinear hydrodynamic PDEs in one and two spatial dimensions, benchmarking short-horizon accuracy, scalability, and long-horizon stability against reference solvers. We empirically characterize the limitations of low-rank approximations with truncation in nonlinear regimes, establishing QTNs as a principled baseline for future physics-informed and data-driven extensions.

Organization of the Paper: The remainder of this paper is organized as follows. Section II reviews the tensor-network preliminaries, including MPS and MPO representations. Section III introduces the proposed QTN framework for tensorized PDE state representation and low-rank one-step operator modeling. Section IV presents the compressed time-stepping methodology and key theoretical properties. Section V reports numerical experiments on linear advection-diffusion and nonlinear viscous Burgers equations in

one and two dimensions. Section VI concludes the paper and outlines future directions.

II. PRELIMINARIES

This section introduces the tensor-network concepts and notation used in this work, focusing on matrix product representations of high-dimensional states (MPS/TT) and operators (MPO/TT-operators).

A. Matrix Product States

Matrix Product States (MPS), also known as tensor trains, provide structured low-rank representations of high-dimensional tensors and originate from quantum many-body physics. In our setting, they serve as a compression framework for tensorized discretized PDE solution fields and for efficient application of structured operators. We summarize the notation and canonical forms used throughout the paper.

1) High-Dimensional States and Tensorization: Let a discretized PDE state sampled on N spatial grid points be represented as a vector $u \in \mathbb{R}^N$. To enable tensor-network compression, we *tensorize* u by reshaping it into an order- n tensor $\psi \in \mathbb{R}^{d \times \dots \times d}$ such that $N = d^n$.¹ Using $s_i \in \{0, 1, \dots, d-1\}$ induces the expansion

$$|\Psi\rangle \in \bigotimes_{i=1}^n \mathbb{R}^d \cong \mathbb{R}^{d^n}, \quad |\Psi\rangle = \sum_{s_1, \dots, s_n} \psi_{s_1 \dots s_n} |s_1\rangle \otimes \dots \otimes |s_n\rangle,$$

where $\{|s_1\rangle \otimes \dots \otimes |s_n\rangle\}$ denotes the tensor-product basis associated with the chosen index encoding of the spatial grid. In the present PDE setting, the indices s_i do not correspond to physical subsystems; they arise solely from the tensorization map.

Although storing ψ still requires $d^n = N$ entries, dense representations of linear maps on this space require $d^{2n} = N^2$ coefficients, and naive operator application and contractions scale accordingly. This motivates representing both states and operators in structured low-rank tensor formats.

2) Matrix Product State Representation: An MPS factorizes the coefficient tensor $\psi_{s_1 \dots s_n}$ into a product of site-local cores:

$$|\Psi\rangle = \sum_{s_1, \dots, s_n} A_1^{(s_1)} A_2^{(s_2)} \dots A_n^{(s_n)} |s_1 \dots s_n\rangle, \quad (1)$$

and equivalently, $\psi_{s_1 \dots s_n} = A_1^{(s_1)} A_2^{(s_2)} \dots A_n^{(s_n)}$, where matrix multiplication over the virtual indices is implied. Each core $A_i^{(s_i)} \in \mathbb{R}^{D_{i-1} \times D_i}$, and (D_0, \dots, D_n) denote the bond dimensions with $D_0 = D_n = 1$.

The total number of parameters scales as $\sum_{i=1}^n D_{i-1} d D_i$. Under a uniform bound $D_i \leq \chi$, this is $O(nd\chi^2)$, i.e., linear in n and polynomial in the maximal bond dimension $\chi = \max_i D_i$. When the bond dimensions remain bounded (or grow slowly) as n increases, this yields substantial compression compared to storing the full tensor of size d^n .

¹If N is not exactly of the form d^n , one may use padding or a mixed-radix tensorization; we restrict to $N = d^n$ for clarity.

3) Canonical Forms: MPS representations are not unique due to gauge freedom: inserting XX^{-1} between adjacent cores leaves the represented tensor unchanged. Canonical forms partially fix this gauge and play a central role in numerical stability and efficient computation [3].

a) Left-canonical form: Applying successive singular value decompositions (SVDs) from left to right yields MPS cores satisfying

$$\sum_{s_i} \left(A_i^{(s_i)} \right)^\top A_i^{(s_i)} = I_{D_i}, \quad (2)$$

where I_D denotes the $D \times D$ identity matrix. This enforces orthonormality on the right virtual index (after reshaping the core into a $(D_{i-1}d) \times D_i$ matrix). Throughout this work, we restrict attention to real-valued tensor networks, so transposition and Hermitian conjugation coincide.

b) Right-canonical form: Applying SVDs from right to left yields cores satisfying

$$\sum_{s_i} A_i^{(s_i)} \left(A_i^{(s_i)} \right)^\top = I_{D_{i-1}}, \quad (3)$$

which enforces orthonormality on the left virtual index (after reshaping the core into a $D_{i-1} \times (dD_i)$ matrix).

c) Mixed-canonical form: For a given central site k , an MPS can be written in mixed-canonical form as

$$|\Psi\rangle = \sum_{s_1, \dots, s_n} A_1^{(s_1)} \dots A_{k-1}^{(s_{k-1})} \Gamma_k^{(s_k)} C_k A_{k+1}^{(s_{k+1})} \dots A_n^{(s_n)} |s_1 \dots s_n\rangle, \quad (4)$$

where the tensors at sites $1, \dots, k-1$ are left-canonical and those at sites $k+1, \dots, n$ are right-canonical. The diagonal (nonnegative) matrix C_k contains the singular values (Schmidt coefficients) associated with the bipartition at bond $(k, k+1)$, and $\Gamma_k^{(s_k)} \in \mathbb{R}^{D_{k-1} \times D_k}$ is the center tensor. Depending on convention, C_k may be absorbed into the center tensor or placed on the adjacent bond; we use the displayed convention for convenience. This form explicitly separates orthonormal left and right blocks and is used to improve conditioning and control bond-dimension growth.

B. Matrix Product Operators

Matrix Product Operators (MPOs) [3], [4] provide a tensor-network representation of linear maps acting on high-dimensional states expressed in MPS form. A linear operator $\mathcal{O} : \mathbb{R}^{d^n} \rightarrow \mathbb{R}^{d^n}$ acts on a state $|\Psi\rangle = \sum_{s'_1, \dots, s'_n} \psi_{s'_1 \dots s'_n} |s'_1 \dots s'_n\rangle$ according to

$$\mathcal{O}|\Psi\rangle = \sum_{s_1, \dots, s_n} \sum_{s'_1, \dots, s'_n} O_{s_1 \dots s_n}^{s'_1 \dots s'_n} \psi_{s'_1 \dots s'_n} |s_1 \dots s_n\rangle, \quad (5)$$

where $O_{s_1 \dots s_n}^{s'_1 \dots s'_n}$ are the coefficients of \mathcal{O} in the tensor-product basis. We use the convention that s' indexes the *input* (column) multi-index and s indexes the *output* (row) multi-index. The full operator tensor has d^{2n} entries and is therefore prohibitively large for large n .

An MPO factorizes the operator tensor into a sequence of site-local cores:

$$O_{s_1 \dots s_n}^{s'_1 \dots s'_n} = \sum_{\alpha_1, \dots, \alpha_{n-1}} W_{1, 1, \alpha_1}^{(s_1, s'_1)} W_{2, \alpha_1, \alpha_2}^{(s_2, s'_2)} \dots W_{n, \alpha_{n-1}, 1}^{(s_n, s'_n)} \quad (6)$$

where each MPO core $W_i \in \mathbb{R}^{R_{i-1} \times d \times d \times R_i}$ with $R_0 = R_n = 1$. For fixed (s_i, s'_i) , the slice $W_i^{(s_i, s'_i)}$ is a matrix in $\mathbb{R}^{R_{i-1} \times R_i}$, and $R = \max_i R_i$ denotes the MPO bond dimension. This factorization exploits low-rank structure to provide compact representations of high-dimensional linear operators.

Remark 1 (Action of an MPO on an MPS): Given an MPS with cores $A_i^{(s_i)} \in \mathbb{R}^{D_{i-1} \times D_i}$, the application of an MPO produces a new MPS whose site tensors are obtained by contracting the physical input index and combining the virtual indices:

$$\tilde{A}_i^{(s_i)} = \sum_{s'_i} W_i^{(s_i, s'_i)} \otimes A_i^{(s'_i)}, \quad (7)$$

where $\tilde{A}_i^{(s_i)} \in \mathbb{R}^{(R_{i-1} D_{i-1}) \times (R_i D_i)}$ and \otimes denotes the Kronecker product over the virtual indices. The resulting bond dimensions reflect the combined ranks of the MPO and MPS and are typically reduced using canonicalization and SVD-based truncation to enforce prescribed bond-dimension limits. In practice, these contractions are implemented using optimized tensor contraction paths to ensure computational efficiency.

Remark 2 (Relevance to PDE Flow Maps): In our framework, the discrete-time PDE update $u^{k+1} = \Phi_{\Delta t}(u^k)$ is represented (after tensorization/encoding) by an MPO acting on an MPS representation of the discretized state. For nonlinear PDEs, this MPO-based one-step update should be interpreted as a low-rank approximation of the one-step map on the states encountered in the rollout. This representation enables compressed operator representation and application in high-dimensional settings by exploiting locality and low-rank structure that often arise in transport and diffusion-dominated regimes.

III. QUANTUM-INSPIRED TENSOR NETWORK (QTN) MODELS

This section introduces the tensor-network representations underlying the proposed framework. We describe how discretized PDE states are encoded as MPS, and how discrete-time flow maps are modeled using structured low-rank operators represented in matrix product operator (MPO) or tensor-train (TT) form.

A. Discretized PDE State Representation

Consider a hydrodynamic PDE defined on a spatial domain $\Omega \subset \mathbb{R}^p$ with solution $u(x, t)$ discretized on a grid of $N = d^n$ points. For clarity, we begin with the one-dimensional case. At time t_k , the discretized state is

$$\mathbf{u}_k = [u(x_0, t_k), u(x_1, t_k), \dots, u(x_{N-1}, t_k)]^\top \in \mathbb{R}^N. \quad (8)$$

Each spatial index $i \in \{0, \dots, N-1\}$ is written in base- d form as $i \equiv (i_1, i_2, \dots, i_n)$ with $i_j \in \{0, 1, \dots, d-1\}$, which induces a tensorization of \mathbf{u}_k into an order- n tensor

$$\mathcal{U}_k(i_1, i_2, \dots, i_n) = \mathbf{u}_k[i] \in \mathbb{R}^{d \times \dots \times d}. \quad (9)$$

(Binary encoding corresponds to the special case $d = 2$.) We denote by $\text{encode} : \mathbb{R}^N \rightarrow \mathbb{R}^{d^n}$ the fixed reshaping map $\mathbf{u}_k \mapsto \Psi_k$, where Ψ_k is the vectorization of \mathcal{U}_k (equivalently, the

coefficient tensor in the tensor-product basis of Section II). The inverse reshaping map is denoted decode , used only for visualization/comparison in experiments.

Following Section II, the tensor \mathcal{U}_k is approximated by an MPS of the form

$$\mathcal{U}_k(i_1, \dots, i_n) \approx \sum_{\alpha_1, \dots, \alpha_{n-1}} A_1^{(i_1)} A_2^{(i_2)} \cdots A_{n-1}^{(i_{n-1})}, \quad (10)$$

where the MPS cores satisfy $A_j^{(i_j)} \in \mathbb{R}^{D_{j-1} \times D_j}$ with $D_0 = D_n = 1$. Canonical forms (left-, right-, and mixed-canonical) are used to improve numerical stability and to control bond-dimension growth.

This construction extends to higher spatial dimensions by mapping a multi-index grid coordinate (e.g., (ℓ_1, \dots, ℓ_p)) to a single base- d index i and then applying the same tensorization; in practice, we choose the index ordering (tensorization architecture) to preserve spatial locality as much as possible.

B. Time-Stepping Operator in Tensorized Coordinates

Let $\mathcal{F}_{\Delta t}$ denote the exact (or reference) discrete-time flow map of the PDE,

$$\mathbf{u}_{k+1} = \mathcal{F}_{\Delta t}(\mathbf{u}_k), \quad (11)$$

which advances the discretized state over a fixed time step Δt . Rather than forming $\mathcal{F}_{\Delta t}$ explicitly as a dense operator on \mathbb{R}^N , we represent and apply a structured low-rank one-step operator in tensorized coordinates using a tensor-network operator \mathcal{T} .

Let $\Psi_k = \text{encode}(\mathbf{u}_k) \in \mathbb{R}^{d^n}$ denote the tensorized representation of the discretized state. The tensor-network time-stepping model is

$$\Psi_{k+1}^{\text{QTN}} = \mathcal{T}(\Psi_k), \quad (12)$$

where $\mathcal{T} : \mathbb{R}^{d^n} \rightarrow \mathbb{R}^{d^n}$ is a linear operator represented as a structured low-rank MPO (equivalently, a TT-operator). The predicted physical state is obtained by decoding:

$$\mathbf{u}_{k+1}^{\text{QTN}} = \text{decode}(\Psi_{k+1}^{\text{QTN}}) = \text{decode}(\mathcal{T}(\Psi_k)). \quad (13)$$

In implementation, applying an MPO to an MPS typically increases intermediate bond dimensions. To control rank growth, we apply canonicalization and SVD-based truncation after each operator application. We denote this (non-differentiable) compression/projection by $\Pi_{\chi_{\max}, \varepsilon_{\text{SVD}}}(\cdot)$, where χ_{\max} is a bond-dimension cap and ε_{SVD} is an SVD threshold. The practical one-step predictor is therefore

$$\mathbf{u}_{k+1}^{\text{QTN}} = \Pi_{\chi_{\max}, \varepsilon_{\text{SVD}}}(\mathcal{T}(\Psi_k)). \quad (14)$$

Although the exact flow map $\mathcal{F}_{\Delta t}$ may be nonlinear, the MPO-based update (14) provides a low-rank *approximation* of the one-step evolution in tensorized coordinates on the states encountered along the rollout. From a numerical perspective, \mathcal{T} can be obtained from a discretization of the PDE (e.g., finite-difference operators assembled in MPO form) and combined with a chosen time-integration scheme (e.g., explicit Euler), while $\Pi_{\chi_{\max}, \varepsilon_{\text{SVD}}}$ controls complexity by preventing uncontrolled rank growth during repeated time stepping.

IV. METHODS

This section details the tensor-network formulation used for approximating discrete-time PDE flow maps via compressed time stepping. Discretized states and operators are represented using MPS and MPO structures, enabling compressed manipulation of high-dimensional dynamics. Tensorization, MPO–MPS application, canonicalization, and bond-dimension truncation are performed within the tensor-network framework. Truncation is treated as a separate (non-differentiable) projection step that controls complexity during rollout.

A. Tensor-Network Time-Stepping Pipeline

Algorithm 1 summarizes the compressed QTN time-stepping loop. Each step applies the MPO update to the current MPS state and truncates the resulting bond dimensions to enforce the prescribed complexity limits.

a) Tensorization and State Encoding: A discretized PDE state $\mathbf{u} \in \mathbb{R}^N$ is tensorized via a fixed index-encoding map (Section II) by reshaping into an order- n tensor with local dimension d , such that $N = d^n$ (binary/QT T corresponds to $d = 2$). The tensor is encoded as an MPS using a prescribed tensorization architecture \mathcal{A} (e.g., sequential, bit-reversed, or locality-preserving layouts). This mapping defines a correspondence between grid indices and MPS sites and is chosen to preserve spatial locality to the extent possible. Encoded states are optionally brought into mixed-canonical form to improve numerical conditioning.

b) Operator Representation: The one-step update in tensorized coordinates is represented as an MPO (TT operator) with cores $W_i \in \mathbb{R}^{R_{i-1} \times d \times d \times R_i}$ and bond dimensions $R_i \leq R_{\max}$. The number of MPO parameters scales as $\sum_{i=1}^n R_{i-1} d^2 R_i = \mathcal{O}(n R_{\max}^2 d^2)$ under uniform rank bounds, enabling compact representations of high-dimensional operators. In practice, such MPOs may arise from a chosen PDE discretization and time-integration scheme (e.g., finite-difference operators assembled in MPO form and combined into a one-step map) [10], [7]. In our experiments, derivative MPOs are constructed from finite-difference stencils; their MPO ranks are therefore fixed by the operator construction.

c) MPO–MPS Application: Given an input MPS $\Psi_k = \text{encode}(\mathbf{u}_k)$, the (pre-compression) next tensorized state is obtained by contracting each MPO core with the corresponding MPS core:

$$\tilde{\Psi}_{k+1} = \mathcal{T}(\Psi_k).$$

This contraction sums over physical indices and combines virtual indices, yielding an MPS whose intermediate bond dimensions typically increase due to the combined MPO and MPS ranks.

d) Canonicalization and Compression: To control rank growth, the predicted MPS is canonicalized and compressed using an SVD-based sweep [3], [4]. At each bond, singular values below a threshold ϵ_{SVD} are discarded and the MPS bond dimension is capped at χ_{\max} . We denote the resulting projection by $\Pi_{\chi_{\max}, \epsilon_{\text{SVD}}}(\cdot)$, where $\Pi_{\chi_{\max}, \epsilon_{\text{SVD}}}$ comprises a canonicalization sweep followed by SVD truncation at each

Algorithm 1 Quantum-Inspired Tensor-Network (QTN) Time Stepping (MPO–MPS with Truncation)

Require: Initial state \mathbf{u}_0 , tensorization architecture \mathcal{A} , one-step MPO \mathcal{T} (for step size Δt , bonds $\leq R_{\max}$), MPS bond cap χ_{\max} , SVD threshold ϵ_{SVD} , number of steps K
Ensure: Rollout $\{\Psi_k^{\text{QTN}}\}_{k=0}^K$ (and optionally $\{\hat{\mathbf{u}}_k\}$)
1: Encode initial state $\Psi_0^{\text{QTN}} \leftarrow \text{encode}(\mathbf{u}_0; \mathcal{A})$.
2: **for** $k = 0$ to $K - 1$ **do**
3: $\tilde{\Psi}_{k+1} \leftarrow \mathcal{T}(\Psi_k^{\text{QTN}})$ {MPO–MPS contraction}
4: $\Psi_{k+1}^{\text{QTN}} \leftarrow \Pi_{\chi_{\max}, \epsilon_{\text{SVD}}}(\tilde{\Psi}_{k+1})$ {canonicalize & truncate}
5: $\hat{\mathbf{u}}_{k+1} \leftarrow \text{decode}(\Psi_{k+1}^{\text{QTN}})$
6: **end for**
7: **return** $\{\Psi_k^{\text{QTN}}\}_{k=0}^K$ (and optionally $\{\hat{\mathbf{u}}_k\}$)

bond. This procedure improves numerical conditioning and prevents uncontrolled rank growth, which is particularly important in transport-dominated or nonlinear regimes.

e) Rollout and Reconstruction: Given an initial condition \mathbf{u}_0 , we iterate the projected one-step map to generate a rollout in tensorized coordinates: $\Psi_{k+1}^{\text{QTN}} = \Pi_{\chi_{\max}, \epsilon_{\text{SVD}}}(\mathcal{T}(\Psi_k^{\text{QTN}}))$, with $\Psi_0^{\text{QTN}} = \text{encode}(\mathbf{u}_0)$. Dense reconstruction $\hat{\mathbf{u}}_k = \text{decode}(\Psi_k^{\text{QTN}})$ is performed only for visualization and for comparison with a reference solver.

Remark 3: The QTN framework serves as a compressed time-stepping baseline for PDE flow maps. Unlike tensor-network learning approaches that identify a time-stepping operator from data, here the one-step MPO \mathcal{T} represents a structured update in tensorized coordinates (e.g., arising from a chosen discretization and time integrator), while $\Pi_{\chi_{\max}, \epsilon_{\text{SVD}}}$ controls complexity by truncating rank growth during rollout. This setting enables a focused assessment of the capabilities and limitations of low-rank tensor networks for scalable PDE time stepping and provides a baseline for future physics-informed or data-driven extensions.

B. Theoretical Properties

The tensor-network formulation employed in this work is grounded in standard linear-algebraic properties of matrix product states and operators. These properties provide structural insight into the proposed QTN models and clarify both their expressive capabilities and intrinsic limitations for PDE time stepping and operator approximation. In particular, they address: (i) representability of tensorized discretized states in MPS/TT form, (ii) local optimality of SVD-based truncation used during compression, and (iii) accumulation of one-step approximation errors under repeated time stepping.

Proposition 1 (Exact MPS/TT representation): Let $\mathbf{u} \in \mathbb{R}^{d^n}$ be any discretized state reshaped into an order- n tensor $\mathcal{U} \in \mathbb{R}^{d \times \dots \times d}$. Then there exists an exact (i.e., without truncation) open-boundary MPS/TT representation of \mathcal{U} with bond dimensions satisfying

$$D_i \leq d^{\min(i, n-i)}, \quad i = 1, \dots, n-1.$$

In particular, any such tensor admits an exact MPS representation with maximal bond dimension at most $d^{\lfloor n/2 \rfloor}$, attained at the cut between sites $\lfloor n/2 \rfloor$ and $\lfloor n/2 \rfloor + 1$.

Proof: The construction follows from successive applications of the singular value decomposition (SVD). First reshape \mathcal{U} into a matrix of size $d \times d^{n-1}$ by grouping indices as (s_1) and (s_2, \dots, s_n) , and perform an SVD:

$$\mathcal{U}_{s_1, (s_2 \dots s_n)} = \sum_{\alpha_1} L_{s_1 \alpha_1} \Sigma_{\alpha_1} R_{\alpha_1, (s_2 \dots s_n)}^\top.$$

Define the first MPS core by $A_1^{(s_1)}[1, \alpha_1] := L_{s_1 \alpha_1}$ and absorb Σ into the remaining tensor $\widehat{\mathcal{U}}_{\alpha_1, (s_2 \dots s_n)}^{(2)} := \Sigma_{\alpha_1} R_{\alpha_1, (s_2 \dots s_n)}^\top$. At step i , reshape the remaining tensor into the unfolding that groups the first i physical indices and the remaining $n-i$ indices, yielding a matrix of size $d^i \times d^{n-i}$, and perform an SVD. The rank of this matrix is at most

$$\min(d^i, d^{n-i}) = d^{\min(i, n-i)},$$

which bounds the bond dimension D_i . The quantity $\min(i, n-i)$ is maximized at $i = \lfloor n/2 \rfloor$, giving $\max_i D_i \leq d^{\lfloor n/2 \rfloor}$. After $n-1$ steps, the full tensor \mathcal{U} is exactly represented as an MPS with the stated bond-dimension bounds. \blacksquare

Proposition 2 (Optimality of SVD-based compression):

Let $X \in \mathbb{R}^{m \times n}$ have singular value decomposition $X = U \Sigma V^\top$, and fix an integer r with $0 \leq r \leq p := \min(m, n)$. Let $X_r = U_r \Sigma_r V_r^\top$ be the rank- r truncation obtained by retaining the r largest singular values. Then X_r is a best rank- r approximation of X in the Frobenius norm, i.e.,

$$\|X - X_r\|_F = \min_{\text{rank}(Y) \leq r} \|X - Y\|_F.$$

In particular, the SVD-based truncation used in MPS/MPO compression is *locally* Frobenius-norm optimal for each matrix unfolding at the moment of truncation (though sequential truncations need not yield a globally optimal tensor-network approximation).

Proof: This result is a direct consequence of the Eckart–Young–Mirsky theorem. Let the singular values of X be $\sigma_1 \geq \sigma_2 \geq \dots \geq \sigma_p \geq 0$, where $p = \min(m, n)$. Then the truncated SVD satisfies $\|X - X_r\|_F^2 = \sum_{i=r+1}^p \sigma_i^2$, and for any matrix Y with $\text{rank}(Y) \leq r$, $\|X - Y\|_F^2 \geq \sum_{i=r+1}^p \sigma_i^2$. Therefore, X_r minimizes the Frobenius norm error among all rank- r approximations of X . \blacksquare

Proposition 3 (Multi-step error propagation): Let $\mathcal{F}_{\Delta t} : \mathbb{R}^N \rightarrow \mathbb{R}^N$ denote the exact discrete-time flow map. Define the implemented QTN one-step predictor in physical space by

$$\widehat{\mathcal{F}}(\mathbf{u}) := \text{decode}(\Pi_{\chi_{\max}, \varepsilon_{\text{SVD}}}(\mathcal{T}(\text{encode}(\mathbf{u})))),$$

where \mathcal{T} is an MPO/TT-operator in tensorized coordinates and $\Pi_{\chi_{\max}, \varepsilon_{\text{SVD}}}$ denotes the canonicalization+truncation projection.

Assume $\mathcal{F}_{\Delta t}$ is Lipschitz on a set $\mathcal{S} \subset \mathbb{R}^N$ containing the exact trajectory $\{\mathbf{u}_k\}_{k \geq 0}$ and the predicted trajectory $\{\mathbf{u}_k^{\text{QTN}}\}_{k \geq 0}$, with constant $L \geq 0$, that is

$$\|\mathcal{F}_{\Delta t}(\mathbf{u}) - \mathcal{F}_{\Delta t}(\mathbf{v})\|_2 \leq L \|\mathbf{u} - \mathbf{v}\|_2, \quad \forall \mathbf{u}, \mathbf{v} \in \mathcal{S}.$$

Define the uniform one-step approximation error on \mathcal{S} as

$$e := \sup_{\mathbf{u} \in \mathcal{S}} \|\widehat{\mathcal{F}}(\mathbf{u}) - \mathcal{F}_{\Delta t}(\mathbf{u})\|_2.$$

Let the exact and QTN rollouts be generated by

$$\mathbf{u}_{k+1} = \mathcal{F}_{\Delta t}(\mathbf{u}_k), \quad \mathbf{u}_{k+1}^{\text{QTN}} = \widehat{\mathcal{F}}(\mathbf{u}_k^{\text{QTN}}), \quad \mathbf{u}_0^{\text{QTN}} = \mathbf{u}_0.$$

Then, for any $m \geq 1$,

$$\|\mathbf{u}_m^{\text{QTN}} - \mathbf{u}_m\|_2 \leq \sum_{j=0}^{m-1} L^j e.$$

Proof: Define $\delta_k := \|\mathbf{u}_k^{\text{QTN}} - \mathbf{u}_k\|_2$. For any $k \geq 0$, add and subtract $\mathcal{F}_{\Delta t}(\mathbf{u}_k^{\text{QTN}})$:

$$\begin{aligned} \delta_{k+1} &= \|\widehat{\mathcal{F}}(\mathbf{u}_k^{\text{QTN}}) - \mathcal{F}_{\Delta t}(\mathbf{u}_k)\|_2 \\ &\leq \|\widehat{\mathcal{F}}(\mathbf{u}_k^{\text{QTN}}) - \mathcal{F}_{\Delta t}(\mathbf{u}_k^{\text{QTN}})\|_2 + \|\mathcal{F}_{\Delta t}(\mathbf{u}_k^{\text{QTN}}) - \mathcal{F}_{\Delta t}(\mathbf{u}_k)\|_2 \\ &\leq e + L \delta_k, \end{aligned}$$

where we used the definition of e and Lipschitz continuity on \mathcal{S} . Since $\delta_0 = 0$, unrolling the recursion yields $\delta_m \leq \sum_{j=0}^{m-1} L^j e$. \blacksquare

Remark 4 (Restart-time bound and interpretation): More generally, if the QTN rollout is initialized at some time k with possibly mismatched state $\mathbf{u}_k^{\text{QTN}} \neq \mathbf{u}_k$, then for any $m \geq 1$,

$$\|\mathbf{u}_{k+m}^{\text{QTN}} - \mathbf{u}_{k+m}\|_2 \leq L^m \|\mathbf{u}_k^{\text{QTN}} - \mathbf{u}_k\|_2 + \sum_{j=0}^{m-1} L^j e.$$

Thus, even small one-step errors can accumulate under repeated time stepping, and the amplification is governed by the Lipschitz constant L of the exact flow map on the relevant trajectory set. In particular, contractive dynamics ($L < 1$) keep QTN errors uniformly bounded, neutral dynamics ($L \approx 1$) lead to at most linear growth with the prediction horizon, and expansive dynamics ($L > 1$) can amplify small discrepancies rapidly.

V. NUMERICAL EXPERIMENTS

This section evaluates the proposed QTN framework for approximating discrete-time PDE flow maps via compressed time stepping. In all experiments, we generate reference solution trajectories using a classical time-integration scheme and compare the QTN rollout against the reference rollout. At inference, we roll out the projected one-step predictor

$$\widehat{\mathcal{F}}(\mathbf{u}) = \text{decode}(\Pi_{\chi_{\max}, \varepsilon_{\text{SVD}}}(\mathcal{T}(\text{encode}(\mathbf{u}))))$$

for multiple steps and compare with the reference. We report qualitative comparisons via snapshots and signed difference plots, and quantify error growth using relative ℓ_2 norms and prediction-horizon curves.

Common tensorization and truncation settings: Unless stated otherwise, we use base- d tensorization with $N = d^n$ (binary/QTT corresponds to $d = 2$), a locality-preserving architecture \mathcal{A} , an MPS bond cap χ_{\max} , an MPO bond cap R_{\max} , and SVD threshold ε_{SVD} . After each MPO application, we apply $\Pi_{\chi_{\max}, \varepsilon_{\text{SVD}}}$ to control rank growth, as described in Section IV.

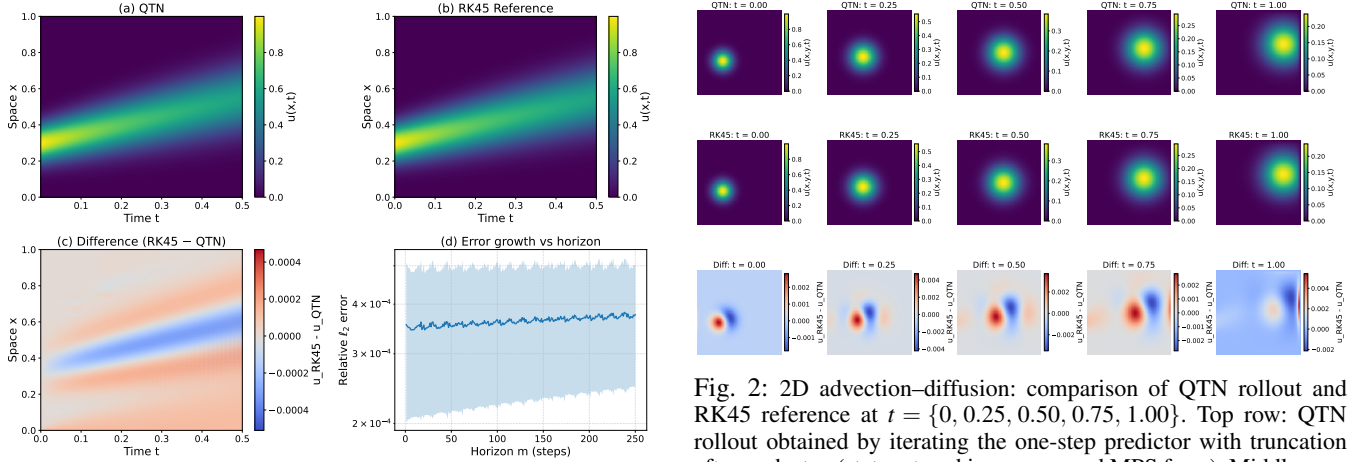


Fig. 1: 1D advection–diffusion: (a) QTN rollout from iterating the one-step MPO predictor with truncation; (b) RK45 reference; (c) signed difference $u_{\text{RK45}} - u_{\text{QTN}}$ (time-aligned); (d) restart-averaged relative ℓ_2 error vs. prediction horizon m .

a) 1D Linear Advection–Diffusion: We consider $u_t + cu_x = vu_{xx}$ on $[0, 1]$ with homogeneous Dirichlet boundary conditions and initial condition $u_0(x) = \exp(-100(x - 0.3)^2)$, using $c = 0.5$, $v = 0.01$, $T = 0.5$, and $N = 2^9 = 512$ grid points. We use an MPS bond cap $\chi_{\max} = 60$ and truncation tolerance $\varepsilon_{\text{SVD}} = 10^{-12}$, applied after each Euler step (after enforcing Dirichlet boundary conditions); the Dirichlet mask MPS is compressed with bond cap 30. Reference trajectories are generated by a method-of-lines discretization (second-order centered differences) and RK45. We implement an MPO-based one-step update \mathcal{T} in tensorized coordinates with binary tensorization ($d = 2$, $n = 9$), applying $\Pi_{\chi_{\max}, \varepsilon_{\text{SVD}}}$ after each MPO application. We then roll out the projected one-step predictor and compare with the RK45 rollout. Figure 1(a–c) shows the QTN rollout, reference, and signed difference $u_{\text{RK45}} - u_{\text{QTN}}$ (time-aligned).

Figure 1(d) reports the restart-averaged relative ℓ_2 error as a function of prediction horizon m . Specifically, for each restart time k , we initialize the QTN model at u_k and measure $\frac{\|u_{k+m}^{\text{QTN}} - u_{k+m}\|_2}{\|u_{k+m}\|_2}$, then average over all valid restart times k . The figure shows small and weakly increasing error, consistent with stable, diffusion-dominated dynamics.

b) 2D Linear Advection–Diffusion: We consider the two-dimensional advection–diffusion equation $u_t + c_x u_x + c_y u_y = v(u_{xx} + u_{yy})$ on $[0, 1]^2$ with homogeneous Dirichlet boundary conditions. We cap the state bond dimension at $\chi_{\max} = 80$ and apply truncation with tolerance $\varepsilon_{\text{SVD}} = 10^{-12}$ after each Euler step (after applying the Dirichlet mask); the boundary mask MPS is compressed with bond cap 40. The initial condition is a Gaussian pulse centered at $(0.3, 0.4)$ with $(c_x, c_y) = (0.5, 0.2)$, $v = 0.01$, final time $T = 1$, and a $2^6 \times 2^6$ grid (total $N = 2^{12}$). Reference trajectories are generated by a method-of-lines discretization (centered finite differences) and RK45. We flatten the 2D grid index and apply a locality-preserving tensorization architecture \mathcal{A} to encode states as MPS, then implement an MPO-based one-

Fig. 2: 2D advection–diffusion: comparison of QTN rollout and RK45 reference at $t = \{0, 0.25, 0.50, 0.75, 1.00\}$. Top row: QTN rollout obtained by iterating the one-step predictor with truncation after each step (states stored in compressed MPS form). Middle row: RK45 reference solution at matching times. Bottom row: signed difference $u_{\text{RK45}} - u_{\text{QTN}}$.

step update \mathcal{T} with truncation via $\Pi_{\chi_{\max}, \varepsilon_{\text{SVD}}}$ after each MPO application. We evaluate multi-step rollouts by iterating the projected one-step predictor and comparing to RK45 in Figure 2. It can be seen that the errors remain spatially smooth over short to moderate horizons, indicating that low-rank MPO updates capture the dominant transport–diffusion dynamics in this regime.

c) 1D Viscous Burgers Equation: To assess performance beyond linear dynamics, we consider the viscous Burgers equation $u_t + uu_x = vu_{xx}$ on $[0, 1]$ with periodic boundary conditions and initial condition $u_0(x) = 1 + 0.5 \sin(2\pi x)$, viscosity $v = 0.01$, and final time $T = 0.5$. The spatial grid uses $N = 2^9$ points. We use an MPS bond cap $\chi_{\max} = 60$ and truncation tolerance $\varepsilon_{\text{SVD}} = 10^{-12}$ applied after each Euler step; periodic boundary conditions are encoded directly in the finite-difference derivative MPOs. A reference solution is computed via method-of-lines discretization with periodic finite differences and RK45 time integration. We implement an MPO-based one-step update \mathcal{T} in tensorized coordinates with truncation after each application. Figure 3 compares QTN rollouts with the RK45 reference, shows the signed difference, and reports restart-averaged relative ℓ_2 error versus prediction horizon m . The signed difference field in Figure 3(c) remains spatially smooth and aligned with the transported wave structure, indicating that discrepancies arise primarily from gradual phase and amplitude mismatch rather than numerical instability or spurious oscillations. Figure 3(d) reports the restart-averaged relative ℓ_2 error versus prediction horizon m , showing more fluctuating error than in the linear advection–diffusion case, reflecting the increased sensitivity of the nonlinear dynamics, yet remaining stable over the tested horizon.

d) 2D Burgers Equation (Periodic): We consider the two-dimensional viscous Burgers equation $u_t + uu_x + uu_y = v(u_{xx} + u_{yy})$ on $[0, 1]^2$ with periodic boundary conditions and viscosity $v = 0.01$, using a 64×64 grid (total $N = 4096 = 2^{12}$) and final time $T = 1$. We use an MPS bond cap $\chi_{\max} = 120$ and truncation tolerance $\varepsilon_{\text{SVD}} = 10^{-12}$ applied after

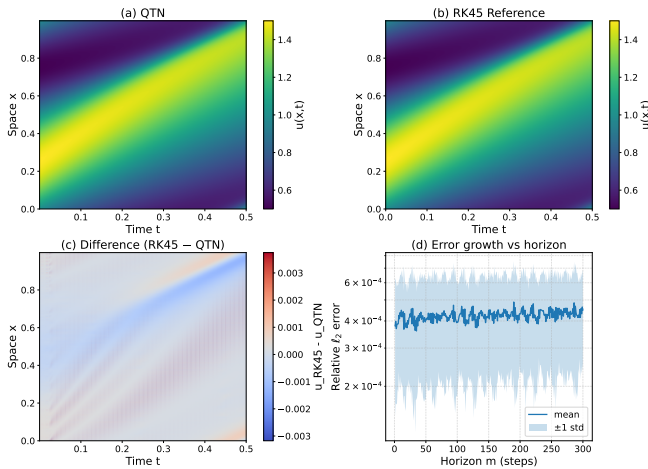


Fig. 3: 1D viscous Burgers (periodic): (a) QTN rollout, (b) RK45 reference, (c) signed difference $u_{\text{RK45}} - u_{\text{QTN}}$ (time-aligned), and (d) restart-averaged relative ℓ_2 error versus prediction horizon m (mean ± 1 std).

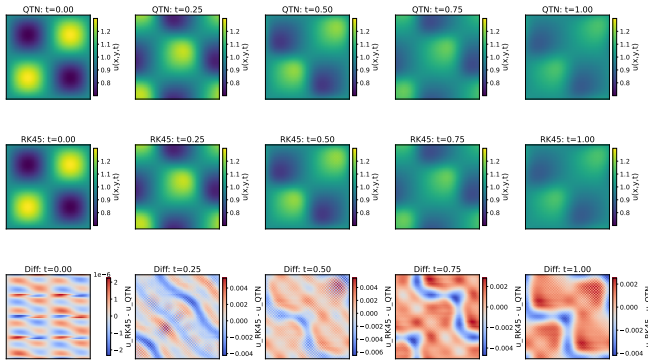


Fig. 4: 2D viscous Burgers: comparison of QTN rollout and RK45 reference at $t = \{0, 0.25, 0.50, 0.75, 1.00\}$. Top row: QTN rollout obtained by iterating the one-step predictor with truncation after each step. Middle row: RK45 reference snapshots at matching times. Bottom row: signed difference $u_{\text{RK45}} - u_{\text{QTN}}$.

each Euler step; periodic boundary conditions are encoded directly in the finite-difference derivative MPOs. Reference trajectories are generated by a method-of-lines discretization with centered finite differences and RK45 time integration. We encode 2D states in MPS form using a locality-preserving tensorization architecture and evaluate multi-step rollouts by iterating the one-step predictor with truncation after each step. Figure 4(a–c) compares the QTN rollout with the RK45 reference and shows the signed difference $u_{\text{RK45}} - u_{\text{QTN}}$ at representative times. The difference fields remain spatially smooth over the shown horizon, while localized discrepancies gradually develop as nonlinear interactions accumulate.

VI. CONCLUSION

We investigated quantum-inspired tensor networks as a fully classical framework for approximating discrete-time flow maps of hydrodynamic PDEs via compressed time stepping. The proposed approach encodes tensorized PDE states in MPS/TT form and represents one-step evolution

updates as low-rank MPO/TT-operators, with rank growth controlled by canonicalization and SVD-based truncation. This yields an interpretable tensor-network baseline that avoids dense representations and does not impose explicit physical constraints (e.g., conservation, reversibility, or unitarity), making it applicable to dissipative dynamics.

Numerical experiments on one- and two-dimensional linear advection–diffusion and viscous Burgers equations show that low-rank MPO updates can accurately capture *short-horizon* dynamics in smooth, diffusion-dominated regimes, while multi-step rollouts exhibit increasing error consistent with accumulated one-step mismatch and compression effects. For nonlinear PDEs, the projected low-rank update should be interpreted as an *approximation* of the one-step map on the states encountered along the rollout, which explains both its effectiveness for local prediction and its limitations for long-horizon extrapolation.

This work establishes quantum-inspired tensor networks as a principled, structured, and scalable baseline for PDE flow-map approximation. Promising future directions include incorporating physics-based inductive biases (e.g., conservation or stability constraints), stability-aware and multi-step objectives, adaptive rank/truncation strategies, and extensions toward data-driven operator identification and hardware-compatible or quantum-motivated parameterizations.

REFERENCES

- [1] B. O. Koopman, “Hamiltonian systems and transformation in hilbert space,” *Proceedings of the National Academy of Sciences*, vol. 17, no. 5, pp. 315–318, 1931.
- [2] S. L. Brunton, J. L. Proctor, and J. N. Kutz, “Discovering governing equations from data by sparse identification of nonlinear dynamical systems,” *Proceedings of the National Academy of Sciences*, vol. 113, no. 15, pp. 3932–3937, 2016.
- [3] U. Schollwöck, “The density-matrix renormalization group in the age of matrix product states,” *Annals of Physics*, vol. 326, no. 1, pp. 96–192, 2011.
- [4] R. Orús, “A practical introduction to tensor networks: Matrix product states and projected entangled pair states,” *Annals of Physics*, vol. 349, pp. 117–158, 2014.
- [5] I. V. Oseledets, “Tensor-train decomposition,” *SIAM Journal on Scientific Computing*, vol. 33, no. 5, pp. 2295–2317, 2011.
- [6] A. Cichocki *et al.*, “Tensor networks for dimensionality reduction and large-scale optimization,” *Foundations and Trends in Machine Learning*, 2016.
- [7] R. D. Peddinti, S. Pisoni, A. Marini, P. Lott, H. Argentieri, E. Tiunov, and L. Aolita, “Quantum-inspired framework for computational fluid dynamics,” *Communications Physics*, vol. 7, no. 1, p. 135, 2024.
- [8] N. Gourianov, M. Lubasch, S. Dolgov, Q. Y. van den Berg, H. Babaee, P. Givi, M. Kiffner, and D. Jaksch, “A quantum-inspired approach to exploit turbulence structures,” *Nature Computational Science*, vol. 2, no. 1, pp. 30–37, 2022.
- [9] M. Kiffner and D. Jaksch, “Tensor network reduced order models for wall-bounded flows,” *Physical Review Fluids*, vol. 8, p. 124101, 2023.
- [10] V. A. Kazeev and B. N. Khoromskij, “Low-rank explicit QTT representation of the laplace operator and its inverse,” *SIAM Journal on Matrix Analysis and Applications*, vol. 33, no. 3, pp. 742–758, 2012.